mathematics

MDPI

Article

An Improved WENO-Z Scheme for Hyperbolic Conservation Laws with New Global Smoothness Indicator

Shuang Han [1] and Mingjun Li [1,2,*]

[1] School of Mathematics and Computational Science, Xiangtan University, Xiangtan 411105, China; shuanghan@smail.xtu.edu.cn
[2] Hunan Key Laboratory for Computation and Simulation in Science and Engineering, Xiangtan University, Xiangtan 411105, China
* Correspondence: limingjun@xtu.edu.cn

Abstract: The fifth-order WENO-Z scheme proposed by Borges et al., using a linear combination of low-order smoothness indicators, is designed to provide a low numerical dissipation to solve hyperbolic conservation laws, while the power q in the framework of WENO-Z plays a key role in its performance. In this paper, a novel global smoothness indicator with fifth-order accuracy, which is based on several lower-order smoothness indicators on two-point sub-stencils, is presented, and a new lower-dissipation WENO-Z scheme (WENO-NZ) is developed. The spectral properties of the WENO-NZ scheme are studied through the ADR method and show that this new scheme can exhibit better spectral results than WENO-Z no matter what the power value is. Accuracy tests confirm that the accuracy of WENO-Z with $q = 1$ would degrade to the fourth order at first-order critical points, while WENO-NZ can recover the optimal fifth-order convergence. Furthermore, numerical experiments with one- and two-dimensional benchmark problems demonstrate that the proposed WENO-NZ scheme can efficiently decrease the numerical dissipation and has a higher resolution compared to the WENO-Z scheme.

Keywords: WENO-Z scheme; smoothness indicator; power parameter; fifth-order convergence; low dissipation; high resolution

MSC: 65M06; 35L65

Citation: Han, S.; Li, M. An Improved WENO-Z Scheme for Hyperbolic Conservation Laws with New Global Smoothness Indicator. *Mathematics* **2023**, *11*, 4449. https://doi.org/10.3390/math11214449

Academic Editor: Hovik Matevossian

Received: 15 September 2023
Revised: 21 October 2023
Accepted: 25 October 2023
Published: 27 October 2023

1. Introduction

As an important class of differential equation, the hyperbolic conservation equation has a wide application in scientific and engineering fields. One of the characteristics of this equation is that the solution may generate discontinuities even if its initial condition is smooth. For capturing the discontinuities, many numerical schemes, such as total variation diminishing schemes (TVD) [1–3], essentially non-oscillatory schemes (ENO) [4–6], weighted essentially non-oscillatory schemes (WENO) [7–10], etc., have been developed in recent decades. Among them, the WENO schemes have attracted great attention because they can not only obtain high-order solutions in smooth regions but also efficiently avoid spurious oscillatory near discontinuities.

The WENO scheme, first proposed by Liu et al. [7], provided one-order higher solutions than the ones of the rth-order ENO scheme [4,5] by using a convex combination of r candidate sub-stencils. Subsequently, Jiang and Shu [8] devised a new smoothness indicator for the WENO scheme by utilizing the Lagrange form of interpolation polynomials and proposed an efficient WENO-JS scheme. For the case $r = 3$, the resulting WENO-JS scheme is about twice as fast as the fourth-order ENO scheme on computational efficiency. Most importantly, this scheme can achieve optimal fifth-order accuracy. Henrick et al. [11] derived a sufficient condition for the fifth-order convergence and conducted a further analysis of the accuracy of WENO-JS. They found that the fifth-order WENO-JS scheme was only

third-order accurate at first-order critical points. To increase the accuracy of the WENO scheme, different types of finite difference WENO schemes by reconstructing flux functions have been proposed [12–16], such as the RBF-WENO scheme, which was based on radial basis functions (RBFs) and the nonlinear weights of WENO-JS, which was first proposed by Guo and Jung in [12] and further developed by Abedian et al. [14,15]. On the other hand, some scholars developed various techniques to calculate the weights to improve the accuracy. For example, Henrick et al. [11] introduced a corrected mapping function to the nonlinear weights of WENO-JS and presented a WENO-M scheme which could restore the optimal convergence order even at critical points but was computationally expensive. Unlike the idea of WENO-M, Borges et al. [9] designed a fifth-order global smoothness indicator using the linear combination of low-order smoothness indicators and proposed an innovative WENO-Z scheme with lower numerical dissipation. Meanwhile, this scheme was able to obtain almost the same accurate numerical solution as WENO-M and reduced computation by 25%.

Castro et al. [17] extended the WENO-Z scheme to arbitrary $(2r-1)$ th odd-order accuracy by designing a general formula for the global smoothness indicator. However, it should be noted that the numerical dissipation of WENO-Z is dependent upon the power parameter q. For example, the scheme is less dissipative with $q = 1$ but will lose accuracy at critical points, such as the fifth-order WENO-Z is only fourth-order accurate at first-order critical points. In contrast, the scheme will decrease the correction of nonlinear weights and is more dissipative with $q = 2$. Hence, Borges et al. [9] suggested the power q taken to be 1 to maintain the low dissipation property. Recently, some studies [18–23] reconstructed a series of higher-order (even up to eighth-order) reference smoothness indicators to recover the optimal convergence for the low-dissipation WENO-Z scheme (means $q = 1$). Although numerical results confirmed that these modified schemes with higher-order smoothness indicators can achieve the desired accuracy in smooth regions including critical points, most of these works either used larger stencils or introduced user-tunable parameters, which led to the increased computation time or limited the application.

On the other hand, Acker et al. [24] concluded the important role of increasing the contribution of less-smooth candidate sub-stencils for increasing the resolution. They added an extra term to WENO-Z weights to increase the relevance of less-smooth sub-stencils and proposed a fifth-order WENO-Z+ scheme. In terms of the lrest progress, a new fifth-order WENO-Z scheme was developed by Tang et al. [25] to perform lower dissipation at discontinuities by constructing a selector that can identify the less-smooth sub-stencils. Unfortunately, the presented WENO schemes in [24,25] were still fourth-order accurate at critical points. Therefore, how to construct a low-dissipation WENO-Z scheme with better performances, which has overall fifth-order accuracy including critical points and a higher resolution near discontinuities, should be investigated thanks to its significant computational benefit.

In this study, we divide the five-point global stencil of the WENO scheme into four smaller two-point sub-stencils. By utilizing the local smoothness indicators of these sub-stencils, we devise a novel fifth-order global smoothness indicator and develop a WENO-NZ scheme. The numerical results demonstrate that the WENO-NZ scheme is less dissipative and can restore the optimal convergence order whatever the value of power q. Additionally, this scheme shows improved capability in capturing discontinuities and small scales and exhibits higher resolution compared to the WENO-Z scheme.

The rest of the paper is structured as follows: In Section 2, a brief overview of the fifth-order WENO-JS and WENO-Z schemes is discussed. In Section 3, an improved WENO-Z scheme is developed by using a new fifth-order global smoothness indicator. The performance comparison between WENO-Z and the proposed scheme for the one- and two-dimensional Euler equations is given in Section 4. Finally, the conclusions are presented in Section 5.

2. Numerical Method

The one-dimensional scalar hyperbolic conservation laws can be written as

$$\frac{\partial u}{\partial t} + \frac{\partial f(u)}{\partial x} = 0,\ x \in [a,\ b],\ t > 0, \tag{1}$$

here, $u(x,\ t)$ is conservative variable, $f(u)$ is flux. Consider the uniform grids $x_j = j\Delta x$ $(j = 0, \cdots, N)$ and define the cell interfaces as $x_{j+1/2} = x_j + \Delta x/2$, Δx is the uniform grid spacing, the semi-discretization of Equation (1) can be given as

$$\frac{du_j}{dt} = -\left(\frac{\partial f}{\partial x}\right)_{x_j}, \tag{2}$$

here, u_j is a numerical approximation to $u\left(x_j,\ t\right)$. The conservation property of Equation (2) is obtained by implicitly defining $f(u) = \frac{1}{\Delta x}\int_{x-\Delta x/2}^{x+\Delta x/2} h(\xi)d\xi$, and have

$$\frac{du_j}{dt} = -\frac{1}{\Delta x}\left(h_{j+1/2} - h_{j-1/2}\right), \tag{3}$$

here, $h_{j\pm1/2} = h\left(x_{j\pm1/2}\right)$. Then, Equation (3) can be further approximated as

$$\frac{du_j}{dt} \approx -\frac{1}{\Delta x}\left(\hat{f}_{j+1/2} - \hat{f}_{j-1/2}\right), \tag{4}$$

here, the numerical fluxes $\hat{f}_{j\pm1/2}$ are higher order polynomial interpolations to $h_{j\pm1/2}$ and can be obtained by the WENO reconstruction.

In general, the flux $f(u)$ is always split into two parts, f^+ and f^-, to ensure numerical stability, such as

$$f(u) = f^+(u) + f^-(u), \tag{5}$$

where $\frac{df^+(u)}{du} \geq 0$ and $\frac{df^-(u)}{du} \leq 0$. In this paper, the global Lax–Friedrichs splitting is used, there are

$$f^{\pm}(u) = \frac{1}{2}(f(u) \pm \alpha u), \tag{6}$$

where $\alpha = \max_u |f'(u)|$. Hence, $\hat{f}^{\pm}_{j+1/2}$ can be computed as the positive and negative parts of $f(u)$, respectively, and have

$$\hat{f}_{j+1/2} = \hat{f}^+_{j+1/2} + \hat{f}^-_{j+1/2}. \tag{7}$$

In fact, $\hat{f}^+_{j+1/2}$ and $\hat{f}^-_{j+1/2}$ are symmetric with respect to $x_{j+1/2}$ for the WENO scheme, so we only describe how $\hat{f}^+_{j+1/2}$ is approximated and the "+" will be dropped in the following content for convenience.

According to the construction of the fifth-order WENO scheme, the numerical flux $\hat{f}_{j+1/2}$ can be given as

$$\hat{f}_{j+1/2} = \sum_{k=0}^{2} \omega_k \hat{f}_{k,j+1/2}, \tag{8}$$

where the numerical fluxes $\hat{f}_{k,j+1/2}(k = 0, 1, 2)$ are given by

$$\begin{aligned}
\hat{f}_{0,j+1/2} &= \tfrac{1}{3}f_{j-2} - \tfrac{7}{6}f_{j-1} + \tfrac{11}{6}f_j, \\
\hat{f}_{1,j+1/2} &= -\tfrac{1}{6}f_{j-1} + \tfrac{5}{6}f_j + \tfrac{1}{3}f_{j+1}, \\
\hat{f}_{2,j+1/2} &= \tfrac{1}{3}f_j + \tfrac{5}{6}f_{j+1} - \tfrac{1}{6}f_{j+2}.
\end{aligned} \tag{9}$$

Now, there are many different WENO construction techniques to compute the nonlinear weights ω_k, while the WENO-JS and WENO-Z are the most popular schemes.

2.1. WENO-JS Scheme

The well-known fifth-order WENO-JS scheme was proposed by Jiang and Shu [8], whose nonlinear weights were defined as

$$\omega_k^{JS} = \frac{\alpha_k^{JS}}{\sum_{k=0}^{2} \alpha_k^{JS}}, \ \alpha_k^{JS} = \frac{d_k}{(\beta_k + \varepsilon)^q}, \tag{10}$$

where d_k are ideal weights that resulted in the fifth-order central upwind scheme, there are $d_0 = 1/10$, $d_1 = 6/10$, and $d_2 = 3/10$ respectively. The power $q \geq 1$ is used to control the weights of less-smooth sub-stencils. The larger the q is set, the smaller the weight is obtained, but the scheme is more dissipative. Hence q = 2 is used for the WENO-JS scheme. ε is a positive sensitivity parameter used to avoid division by 0 and $\varepsilon = 10^{-40}$ is adopted in this study. The local smoothness indicator β_k is defined by

$$\beta_k = \sum_{l=1}^{r-1} \Delta x^{2l-1} \int_{x_{j-1/2}}^{x_{j+1/2}} \left(\frac{d^l}{dx^l} \hat{f}_k(x) \right)^2 dx. \tag{11}$$

For the fifth-order WENO scheme (r = 3), the β_k can be further expressed as

$$\begin{aligned} \beta_0 &= \tfrac{13}{12}\left(f_{j-2} - 2f_{j-1} + f_j\right)^2 + \tfrac{1}{4}\left(f_{j-2} - 4f_{j-1} + 3f_j\right)^2, \\ \beta_1 &= \tfrac{13}{12}\left(f_{j-1} - 2f_j + f_{j+1}\right)^2 + \tfrac{1}{4}\left(f_{j+1} - f_{j-1}\right)^2, \\ \beta_2 &= \tfrac{13}{12}\left(f_j - 2f_{j+1} + f_{j+2}\right)^2 + \tfrac{1}{4}\left(3f_j - 4f_{j+1} + f_{j+2}\right)^2. \end{aligned} \tag{12}$$

The Taylor expansions of Equation (12) at x_j can be given as

$$\begin{aligned} \beta_0 &= {f'}_j^2 \Delta x^2 + \left(\tfrac{13}{12} {f''}_j^2 - \tfrac{2}{3} {f'}_j {f'''}_j\right)\Delta x^4 - \left(\tfrac{13}{6} {f''}_j {f'''}_j - \tfrac{1}{2} {f'}_j f_j^{(4)}\right)\Delta x^5 + O\left(\Delta x^6\right), \\ \beta_1 &= {f'}_j^2 \Delta x^2 + \left(\tfrac{13}{12} {f''}_j^2 + \tfrac{1}{3} {f'}_j {f'''}_j\right)\Delta x^4 + O\left(\Delta x^6\right), \\ \beta_2 &= {f'}_j^2 \Delta x^2 + \left(\tfrac{13}{12} {f''}_j^2 - \tfrac{2}{3} {f'}_j {f'''}_j\right)\Delta x^4 + \left(\tfrac{13}{6} {f''}_j {f'''}_j - \tfrac{1}{2} {f'}_j f_j^{(4)}\right)\Delta x^5 + O\left(\Delta x^6\right). \end{aligned} \tag{13}$$

Substituting Equation (13) into Equation (10), there are

$$\begin{cases} \omega_k^{JS} = d_k + O\left(\Delta x^2\right), \ {f'}_j \neq 0, \\ \omega_k^{JS} = d_k + O(\Delta x), \ \ {f'}_j = 0, \ {f_j}'' \neq 0. \end{cases} \tag{14}$$

Henrick et al. [11] concluded a detailed analysis of the accuracy of the fifth-order WENO scheme and derived a sufficient condition for the fifth-order convergence as follows

$$\omega_k - d_k = O\left(\Delta x^3\right). \tag{15}$$

Equation (15) is further weakened as $\omega_k - d_k = O\left(\Delta x^2\right)$ by Don et al. in [26]. Although it is not a necessary condition, it can be used as a simple criterion for designing nonlinear weights. Obviously, the weights of WENO-JS cannot meet the sufficient condition of Equation (15), especially at first-order critical points. It was reported that the WENO-JS scheme was only third-order accurate at critical points [11].

2.2. WENO-Z Scheme

Borges et al. [9] developed another fifth-order WENO scheme, called WENO-Z. They defined the nonlinear weights as

$$\omega_k^Z = \frac{\alpha_k^Z}{\sum_{k=0}^{2} \alpha_k^Z}, \ \alpha_k^Z = d_k\left(1 + \left(\frac{\tau_5}{\beta_k + \varepsilon}\right)^q\right), \ q = 1, 2. \tag{16}$$

Here, τ_5 is a global smoothness indicator given as

$$\tau_5 = |\beta_0 - \beta_2|, \tag{17}$$

which with the following Taylor expansion

$$\tau_5 = \left|\frac{13}{3} f''_j f'''_j - f'_j f_j^{(4)}\right| \Delta x^5. \tag{18}$$

Substituting Equations (13) and (18) into Equation (16), then have

$$\begin{cases} \omega_k^Z = d_k + O\left(\Delta x^{3q}\right), \ f'_j \neq 0, \\ \omega_k^Z = d_k + O(\Delta x^q), \ f'_j = 0, \ f_j'' \neq 0. \end{cases} \tag{19}$$

It can be found that the weights of WENO-Z with $q = 1$ do not meet the sufficient condition (15) at first-order critical points. Furthermore, Borges et al., confirmed that the WENO-Z scheme with $q = 2$ achieved fifth-order accuracy even at critical points. However, an increase in q resulted in more numerical dissipation of WENO-Z. Therefore, the power parameter $q = 1$ is suggested by Borges et al. and used by other scholars [18–25].

3. The New WENO-Z Scheme

Some works [20–23] demonstrated that constructing more higher-order smoothness indicators was useful in recovering the desired order for the low-dissipation WENO-Z scheme (means $q = 1$). Unlike these studies, we reconstructed a novel fifth-order global smoothness indicator with lower dissipation for the WENO-Z scheme to overcome its inherent limitations, such as its failure to balance the low-dissipation property and fifth-order convergence.

3.1. Construction of Novel Global Smoothness Indicator

Within the framework for the original global smoothness indicator τ_5 of WENO-Z, it is found that a discontinuity would affect the interpolation on the range of $2\Delta x$ at least. Suppose a discontinuity is at any position to the left (or right) side of the center point x_j, it would affect the interpolation on the three-point sub-stencil S_0 (or S_2). However, if a discontinuity is just right at x_j, it would affect the interpolation of the entire five-point global stencil. To reduce the impact of the discontinuities on interpolation, we subdivided the global stencil into four smaller sub-stencils $\{S_{00}, S_{01}, S_{12}, S_{22}\}$, each one only involving two points, as shown in Figure 1. In fact, these sub-stencils are generally used to construct the third-order WENO-Z scheme ($r = 2$).

Based on these new smaller sub-stencils, a discontinuity will affect the nearby $2\Delta x$ range at most, that is, two two-point sub-stencils. Furthermore, only a two-point sub-stencil where the discontinuity is located may be affected. From Equation (11), the smoothness indicators on sub-stencils $\{S_{00}, S_{01}, S_{12}, S_{22}\}$ can be computed as

$$\beta_{00} = (f_{i-2} - f_{i-1})^2, \ \beta_{01} = (f_{i-1} - f_i)^2, \ \beta_{12} = (f_i - f_{i+1})^2, \ \beta_{22} = (f_{i+1} - f_{i+2})^2, \tag{20}$$

with the following Taylor expansions

$$\begin{aligned}
\beta_{00} &= f'^2_j\Delta x^2 - 3f'_jf''_j\Delta x^3 + \left(\tfrac{9}{4}f''^2_j + \tfrac{7}{3}f'_jf'''_j\right)\Delta x^4 - \left(\tfrac{7}{2}f''_jf'''_j + \tfrac{5}{4}f'_jf^{(4)}_j\right)\Delta x^5 + O(\Delta x^6),\\
\beta_{01} &= f'^2_j\Delta x^2 - f'_jf''_j\Delta x^3 + \left(\tfrac{1}{4}f''^2_j + \tfrac{1}{3}f'_jf'''_j\right)\Delta x^4 - \left(\tfrac{1}{6}f''_jf'''_j + \tfrac{1}{12}f'_jf^{(4)}_j\right)\Delta x^5 + O(\Delta x^6),\\
\beta_{12} &= f'^2_j\Delta x^2 + f'_jf''_j\Delta x^3 + \left(\tfrac{1}{4}f''^2_j + \tfrac{1}{3}f'_jf'''_j\right)\Delta x^4 + \left(\tfrac{1}{6}f''_jf'''_j + \tfrac{1}{12}f'_jf^{(4)}_j\right)\Delta x^5 + O(\Delta x^6),\\
\beta_{22} &= f'^2_j\Delta x^2 + 3f'_jf''_j\Delta x^3 + \left(\tfrac{9}{4}f''^2_j + \tfrac{7}{3}f'_jf'''_j\right)\Delta x^4 + \left(\tfrac{7}{2}f''_jf'''_j + \tfrac{5}{4}f'_jf^{(4)}_j\right)\Delta x^5 + O(\Delta x^6).
\end{aligned} \tag{21}$$

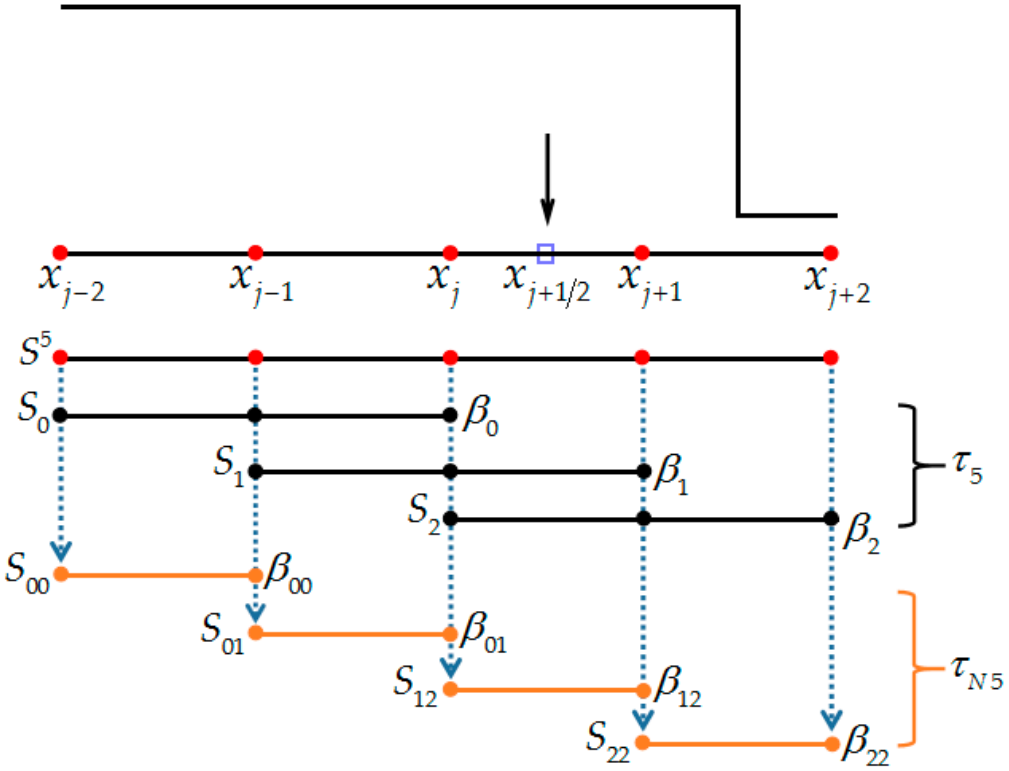

Figure 1. The construction stencils of the new global smoothness indicator.

Consider the WENO scheme will lose accuracy at first-order critical points, in order to minimize the influence of the first-order derivative, meanwhile ensuring the global smoothness indicator has high-order accuracy, the form of a new fifth-order global smoothness indicator can be given as

$$\tau_{N5} = |\beta_{00} - 3\beta_{01} + 3\beta_{12} - \beta_{22}|/6, \tag{22}$$

the Taylor expansion of τ_{N5} is as follows

$$\tau_{N5} = \left|f_j''f_j''' + \frac{1}{3}f_j'f_j^{(4)}\right|\Delta x^5. \tag{23}$$

3.1.1. Accuracy

Based on the nonlinear weights for the WENO-Z scheme, substituting τ_{N5} instead of τ_5 into Equation (16) can obtain a new weight, as follows

$$\omega_k^{NZ} = \frac{\alpha_k^{NZ}}{\sum_{k=0}^{2}\alpha_k^{NZ}},\ \alpha_k^{NZ} = d_k\left(1 + \left(\frac{\tau_{N5}}{\beta_k + \varepsilon}\right)^q\right),\ q = 1, 2. \tag{24}$$

Substituting Equation (24) into Equation (8) results in a new WENO scheme, which is named WENO-NZ in this paper. Since τ_{N5} has the same fifth-order accuracy as τ_5, similar to the accuracy analysis of WENO-Z, there are

$$\omega_k^{NZ} = \begin{cases} d_k + O\left(\Delta x^{3q}\right), \ f'_j \neq 0, \\ d_k + O(\Delta x^q), \ f'_j = 0, \ f_j'' \neq 0, \end{cases} \tag{25}$$

which indicates that the WENO-NZ scheme has the same theoretical convergence accuracy as WENO-Z. A detailed analysis of the accuracy properties can be found in [9]. For simplicity, the WENO-Z and WENO-NZ schemes with different powers (q = 1 or 2) are, respectively, denoted as WENO-Z1, WENO-Z2, WENO-NZ1, and WENO-NZ2 in this paper.

3.1.2. Weights of Less-Smooth Sub-Stencils

In [9], numerical results made evident that the WENO-Z places higher weights on less-smooth sub-stencils than WENO-JS, this is the reason why WENO-Z achieves less dissipative results. The results in [24] also showed that it is important to increase the weights of less-smooth sub-stencils. Therefore, here is a numerical example to analyze the weights of less-smooth sub-stencils for the new WENO-NZ scheme.

Consider the linear case of Equation (1) as follows

$$u(x, t = 0) = f(x) = \begin{cases} -\sin(\pi x) - \frac{1}{2}x^3, & -1 \leq x < 0, \\ -\sin(\pi x) - \frac{1}{2}x^3 + 1, & 0 \leq x \leq 1, \end{cases} \tag{26}$$

with the exact solution $u(x,t) = u(x-t,0)$. This numerical example contains a jump discontinuity at x = 0, which is usually used to study the behavior of nonlinear weights in the smooth and discontinuous regions for the WENO scheme. We compute this numerical example to the final time t = 2.0 using N = 200 with periodic boundary, and the time step is set as $\Delta t = \Delta x/2$. As shown in Figure 2a, the numerical results of WENO-NZ1 are the closest to that of the exact solution, and WENO-Z2 generates the most dissipation near discontinuities compared to others. Figure 2b gives the values of smoothness indicators at the initial step t = 0, i.e., $\beta_k (k = 0, 1, 2)$, τ_5, and τ_{N5}. We can see that τ_{N5} is smaller than τ_5 whether in smooth or discontinuous regions, hence, the WENO-NZ scheme is more accurate compared to WENO-Z.

Figure 3 further provides the distributions of nonlinear weights for WENO-Z1, WENO-Z2, WENO-NZ1, and WENO-NZ2. As Figure 3 shows, at the point $x = -0.02$, where the discontinuity occurs for the first time, the ω_2 is smaller than ω_0 and ω_1, that is, the nonlinear weight of the less-smooth sub-stencil is smaller than that of smooth ones. It can be seen that the WENO-NZ assigns relatively larger weights to the less-smooth sub-stencils compared to the corresponding WENO-Z scheme. It can also be seen that the nonlinear weights of the WENO-NZ scheme are nearer to the ideal ones, resulting in the WENO-NZ scheme being closer to the central upwind scheme. As a result, this new scheme is less dissipative than the WENO-Z scheme.

3.2. The Spectral Properties of New Scheme

The spectral properties of the WENO-NZ scheme are studied using the ADR method proposed by Pirozzoli in [27]. As shown in Figure 4, it can be found that the dispersion and dissipation results of the WENO-NZ scheme are closer to the fifth-order upwind scheme (UP5) compared to WENO-Z, and the dispersion and dissipation curves of WENO-NZ are very similar to those of UP5. In addition, the spectral results of WENO-Z1 are better than those of WENO-Z2, but the results of WENO-NZ2 are nearly equivalent to that of WENO-NZ1, which implies that compared to WENO-Z, the WENO-NZ is a lower-dissipation scheme regardless of power q.

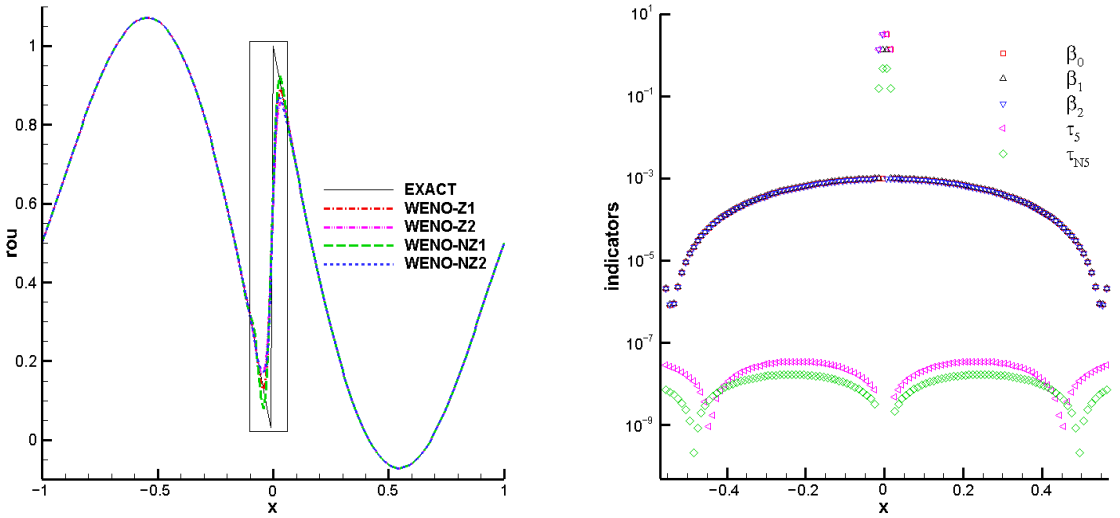

(**a**) (**b**)

Figure 2. Numerical solutions of the linear equation with discontinuity computed by different WENO schemes; (**a**) density distribution; (**b**) the values of smoothness indicators at $t = 0$.

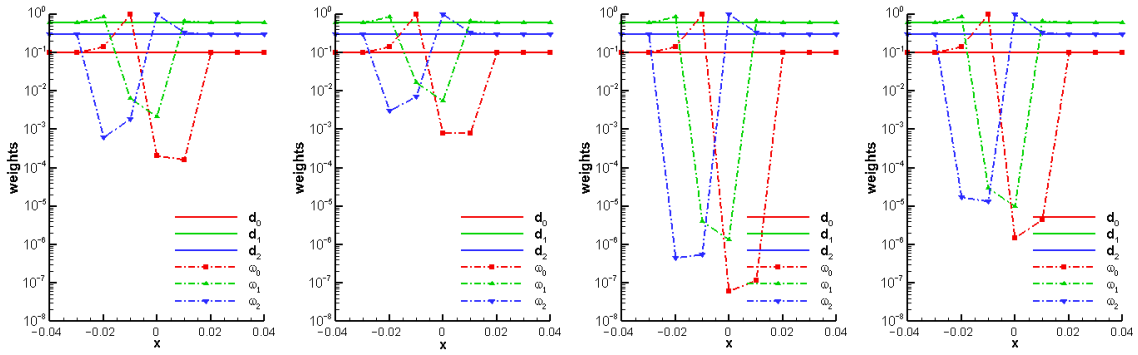

(**a**) (**b**) (**c**) (**d**)

Figure 3. The nonlinear weights of different schemes for the linear equation with discontinuity at $t = 0$; (**a**) WENO-Z1; (**b**) WENO-NZ1; (**c**) WENO-Z2; (**d**) WENO-NZ2.

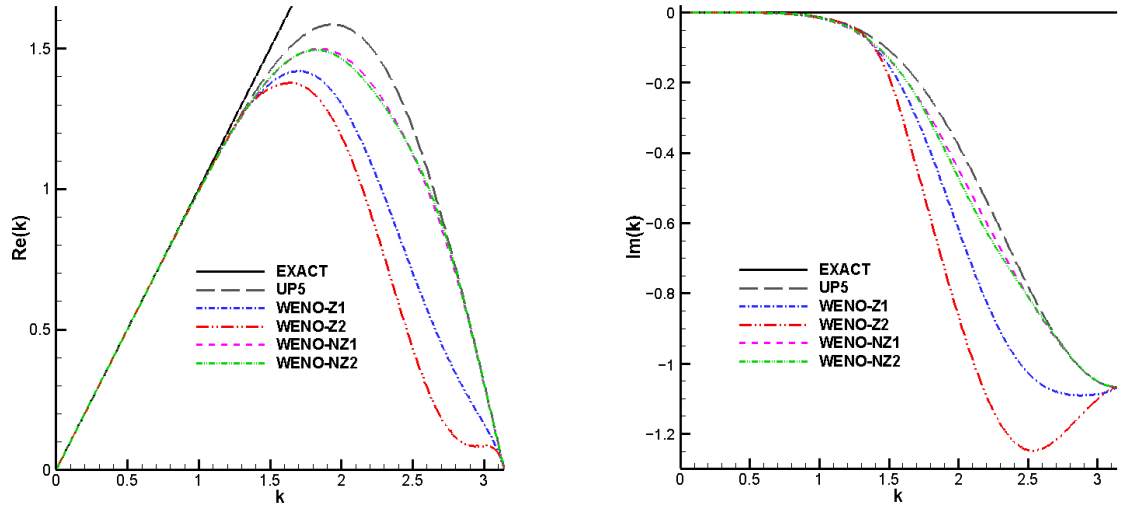

(**a**) (**b**)

Figure 4. The dispersion and dissipation properties of WENO-Z and WENO-NZ schemes; (**a**) dispersion; (**b**) dissipation.

4. Numerical Results

In this section, a series of typical numerical examples involving discontinuities and complex scale waves are computed to examine the accuracy, resolution, and low-dissipation properties of the proposed WENO-NZ scheme. The third-order Runge–Kutta method [1] is applied for time discretization with a CFL number of 0.5, as

$$\begin{aligned} u^{(1)} &= u^n + \Delta t L[u^n], \\ u^{(2)} &= \tfrac{3}{4}u^n + \tfrac{1}{4}\left(u^{(1)} + \Delta t L\left[u^{(1)}\right]\right), \\ u^{(3)} &= \tfrac{1}{3}u^n + \tfrac{2}{3}\left(u^{(2)} + \Delta t L\left[u^{(2)}\right]\right), \end{aligned} \tag{27}$$

where L is the spatial operator.

4.1. Linear Advection Problems

Consider the following linear advection problems

$$\begin{cases} \frac{\partial u}{\partial t} + \frac{\partial u}{\partial x} = 0, & x \in [a, b], \\ u(x, t = 0) = u_0(x), & \text{periodic boundary}, \end{cases} \tag{28}$$

with the exact solution $u(x, t) = u_0(x - t)$.

4.1.1. Accuracy Test

Case 1. The smooth initial condition is given as

$$u_0(x) = \sin(\pi x), \ -1 \le x \le 1. \tag{29}$$

This solution is computed up to t = 2.0 using the grids N = 40, 80, 160, 320, 640, and 1280. The time step is set as $\Delta x^{5/4}$. In Table 1, the L^1, L^2, and L^∞ errors, convergence orders, and CPU times are exhibited for the WENO-Z and WENO-NZ schemes with different powers, respectively. Here, the norm of errors is computed by

$$\begin{aligned} L_1 &= \frac{1}{N}\sum_{j=1}^{N}\left|u_j - (u_{exact})_j\right|, \\ L_2 &= \sqrt{\frac{1}{N}\sum_{j=1}^{N}\left(u_j - (u_{exact})_j\right)^2}, \\ L_\infty &= \max_{1\le j\le N}\left|u_j - (u_{exact})_j\right|. \end{aligned} \tag{30}$$

It can be seen that all schemes can achieve fifth-order accuracy, but the CPU time of WENO-Z1 is the shortest compared to other schemes.

Case 2. The second initial condition for the accuracy test is given as

$$u_0(x) = \sin\left(\pi x - \frac{\sin(\pi x)}{\pi}\right), \ -1 \le x \le 1. \tag{31}$$

This solution has two critical points. We compute the solution up to t = 2.0 using the grids N = 40, 80, 160, 320, 640, and 1280 with $\Delta t = \Delta x^{5/4}$. The L^1, L^2, and L^∞ errors, convergence orders, and CPU times for different schemes are exhibited in Table 2. It can be found that the L^∞ errors of WENO-Z2, WENO-NZ1, and WENO-NZ2 are one order of magnitude lower than WENO-Z1. For ease of observation, Figure 5 gives the line graphs of L^∞ errors and orders. From Figure 5a, it can be seen that the L^∞ errors of WENO-Z2, WENO-NZ1, and WENO-NZ2 are almost the same and are smaller than those of WENO-Z1. Moreover, it can also be seen from Figure 5b that the L^∞ order of WENO-Z1

is only fourth-order accurate with the increase in grid numbers, while other schemes can achieve the desired fifth-order accuracy. Therefore, WENO-NZ proves to be a precise and effective scheme.

Table 1. The errors, orders, and CPU times for linear advection problem with smooth initial condition computed by different WENO schemes.

Method	N	L^1 Error	Order	L^2 Error	Order	L^∞ Error	Order	Time
WENO-Z1	40	6.4906×10^{-6}	---	7.3342×10^{-6}	---	1.0792×10^{-5}	---	0.09360
	80	2.0181×10^{-7}	5.01	2.2523×10^{-7}	5.09	3.2397×10^{-7}	5.06	0.31200
	160	6.3021×10^{-9}	5.00	7.0126×10^{-9}	5.03	9.9715×10^{-9}	5.02	1.23241
	320	1.9695×10^{-10}	5.00	2.1894×10^{-10}	5.01	3.1007×10^{-10}	5.01	5.44443
	640	6.1552×10^{-12}	5.00	6.8396×10^{-12}	5.00	9.6797×10^{-12}	5.00	25.02256
	1280	1.9237×10^{-13}	5.00	2.1371×10^{-13}	5.00	3.0235×10^{-13}	5.00	117.01635
WENO-Z2	40	6.4581×10^{-6}	---	7.2051×10^{-6}	---	1.0281×10^{-5}	---	0.10920
	80	2.0168×10^{-7}	5.00	2.2462×10^{-7}	5.00	3.1934×10^{-7}	5.01	0.24960
	160	6.3015×10^{-9}	5.00	7.0101×10^{-9}	5.00	9.9414×10^{-9}	5.01	1.21681
	320	1.9694×10^{-10}	5.00	2.1893×10^{-10}	5.00	3.1006×10^{-10}	5.00	5.55364
	640	6.1552×10^{-12}	5.00	6.8396×10^{-12}	5.00	9.6797×10^{-12}	5.00	24.96016
	1280	1.9237×10^{-13}	5.00	2.1371×10^{-13}	5.00	3.0235×10^{-13}	5.00	120.44837
WENO-NZ1	40	6.4712×10^{-6}	---	7.2545×10^{-6}	---	1.0476×10^{-5}	---	0.03120
	80	2.0173×10^{-7}	5.00	2.2486×10^{-7}	5.01	3.2110×10^{-7}	5.03	0.37440
	160	6.3017×10^{-9}	5.00	7.0111×10^{-9}	5.001	9.9534×10^{-9}	5.01	1.40401
	320	1.9694×10^{-10}	5.00	2.1893×10^{-10}	5.00	3.1006×10^{-10}	5.00	6.30244
	640	6.1552×10^{-12}	5.00	6.8396×10^{-12}	5.00	9.6797×10^{-12}	5.00	29.37499
	1280	1.9237×10^{-13}	5.00	2.1371×10^{-13}	5.00	3.0235×10^{-13}	5.00	136.98448
WENO-NZ2	40	6.4580×10^{-6}	---	7.2028×10^{-6}	---	1.0281×10^{-5}	---	0.15600
	80	2.0168×10^{-7}	5.00	2.2462×10^{-7}	5.00	3.1934×10^{-7}	5.01	0.35880
	160	6.3015×10^{-9}	5.00	7.0101×10^{-9}	5.00	9.9414×10^{-9}	5.01	1.41961
	320	1.9694×10^{-10}	5.00	2.1893×10^{-10}	5.00	3.1006×10^{-10}	5.00	6.17764
	640	6.1552×10^{-12}	5.00	6.8396×10^{-12}	5.00	9.6797×10^{-12}	5.00	29.46859
	1280	1.9237×10^{-13}	5.00	2.1371×10^{-13}	5.00	3.0235×10^{-13}	5.00	138.91889

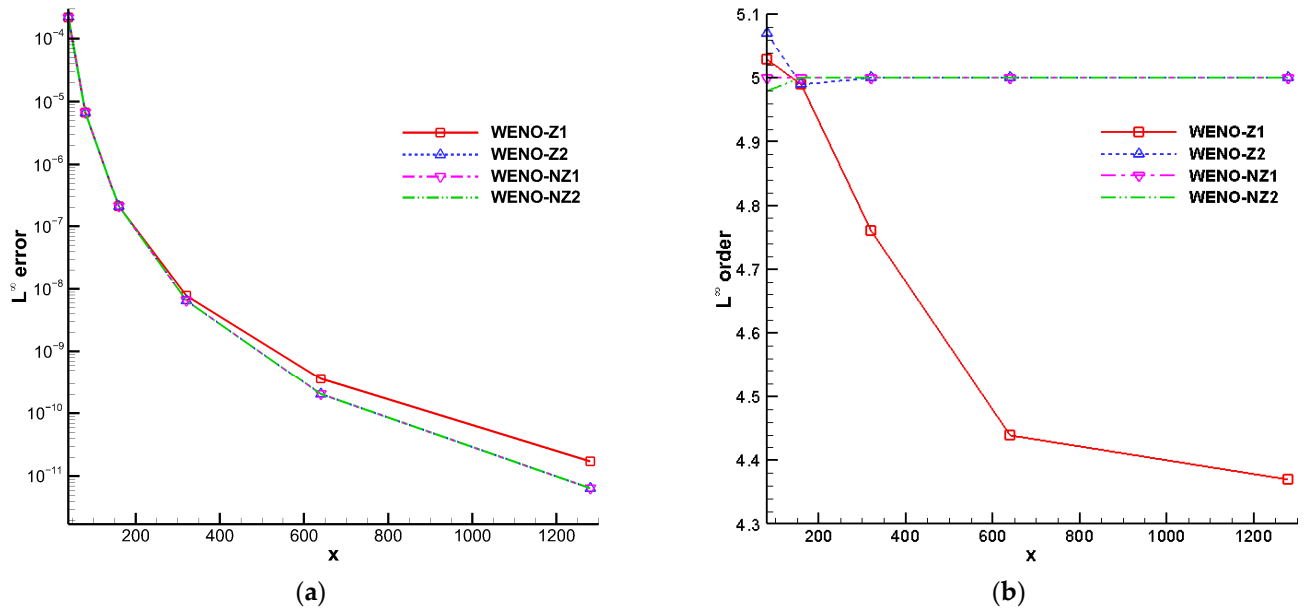

(**a**) (**b**)

Figure 5. The numerical results for the linear advection problem with two critical points computed by different WENO schemes; (**a**) L^∞ errors; (**b**) L^∞ orders.

Table 2. The errors, orders, and CPU times for the linear advection problem with two critical points were computed by different WENO schemes.

Method	N	L^1 Error	Order	L^2 Error	Order	L^∞ Error	Order	Time
WENO-Z1	40	7.0429×10^{-5}	---	9.5195×10^{-5}	---	2.1744×10^{-4}	---	0.06240
	80	2.4102×10^{-6}	4.87	3.1785×10^{-6}	4.90	6.6772×10^{-6}	5.03	0.28080
	160	7.8990×10^{-8}	4.93	1.0142×10^{-7}	4.97	2.0989×10^{-7}	4.99	1.12321
	320	2.5157×10^{-9}	4.97	3.2185×10^{-9}	4.98	7.7672×10^{-9}	4.76	5.60044
	640	7.8219×10^{-11}	5.00	1.0239×10^{-10}	4.97	3.5698×10^{-10}	4.44	25.47496
	1280	2.4235×10^{-12}	5.01	3.2682×10^{-12}	4.97	1.7250×10^{-11}	4.37	118.74796
WENO-Z2	40	6.6140×10^{-5}	---	9.2603×10^{-5}	---	2.2383×10^{-4}	---	0.09360
	80	2.2447×10^{-6}	4.88	3.0595×10^{-6}	4.92	6.6812×10^{-6}	5.07	0.37440
	160	7.2388×10^{-8}	4.95	9.6470×10^{-8}	4.99	2.0987×10^{-7}	4.99	1.23241
	320	2.2821×10^{-9}	4.99	3.0181×10^{-9}	5.00	6.5525×10^{-9}	5.00	5.46004
	640	7.1426×10^{-11}	5.00	9.4316×10^{-11}	5.00	2.0464×10^{-10}	5.00	26.31737
	1280	2.2327×10^{-12}	5.00	2.9471×10^{-12}	5.00	6.3923×10^{-12}	5.00	121.25958
WENO-NZ1	40	7.1643×10^{-5}	---	9.5751×10^{-5}	---	2.1375×10^{-4}	---	0.12480
	80	2.2953×10^{-6}	4.96	3.0766×10^{-6}	4.96	6.6998×10^{-6}	5.00	0.48360
	160	7.2863×10^{-8}	4.98	9.6755×10^{-8}	4.99	2.0990×10^{-7}	5.00	1.27921
	320	2.3087×10^{-9}	4.98	3.0290×10^{-9}	5.00	6.5526×10^{-9}	5.00	6.22444
	640	7.2598×10^{-11}	4.99	9.4765×10^{-11}	5.00	2.0464×10^{-10}	5.00	28.90699
	1280	2.2695×10^{-12}	5.00	2.9652×10^{-12}	5.00	6.3923×10^{-12}	5.00	137.24968
WENO-NZ2	40	7.3503×10^{-5}	---	9.6607×10^{-5}	---	2.1206×10^{-4}	---	0.07800
	80	2.3293×10^{-6}	4.98	3.0796×10^{-6}	4.97	6.7004×10^{-6}	4.98	0.35880
	160	7.3012×10^{-8}	5.00	9.6541×10^{-8}	5.00	2.0988×10^{-7}	5.00	1.48201
	320	2.2852×10^{-9}	5.00	3.0181×10^{-9}	5.00	6.5526×10^{-9}	5.00	6.31804
	640	7.1435×10^{-11}	5.00	9.4313×10^{-11}	5.00	2.0464×10^{-10}	5.00	29.28139
	1280	2.2327×10^{-12}	5.00	2.9471×10^{-12}	5.00	6.3923×10^{-12}	5.00	139.57409

4.1.2. Linear Problem with Several Critical Points

The initial condition is given as

$$u_0(x) = e^{-(x-90)^2/400}\left(\cos\left(\frac{\pi}{8}(x-90)\right) + \cos\left(\frac{\pi}{4}(x-90)\right)\right),\ 50 \le x \le 130. \tag{32}$$

This solution involves several critical points and is often used to test the numerical dissipation of WENO schemes. The solution is calculated by using $N = 100$ until the final time $t = 400$ with $\Delta t = \Delta x/2$. As Figure 6 shows, the numerical results of WENO-NZ are closer to the exact solution than WENO-Z, which again reveals that the WENO-NZ is a lower-dissipation scheme. In addition, the numerical results of WENO-NZ2 are almost comparable or even better than those of WENO-NZ1 at critical points, this is because the weights of WENO-NZ1 cannot satisfy the fifth-order convergence sufficient condition at critical points, but WENO-NZ2 can satisfy and also provide the lower dissipation.

4.2. One-Dimensional Euler Problems

The one-dimensional Euler equation can be written as

$$\frac{\partial \mathbf{U}}{\partial t} + \frac{\partial \mathbf{F}(\mathbf{U})}{\partial x} = 0, \tag{33}$$

with

$$\mathbf{U} = \begin{pmatrix} \rho \\ \rho u \\ E \end{pmatrix}, \mathbf{F}(\mathbf{U}) = \begin{pmatrix} \rho u \\ \rho u^2 + p \\ u(E+p) \end{pmatrix}. \tag{34}$$

Here,ρ, p, u, and E are the density, pressure, x-velocity, and total energy, respectively. The total energy is given as $E = \frac{p}{\gamma-1} + \frac{1}{2}\rho u^2$ with the ratio of specific heat $\gamma = 1.4$. In this

subsection, the extrapolation boundary conditions are adopted and the "exact" solution is computed using the fifth-order WENO-JS scheme with $N = 2000$.

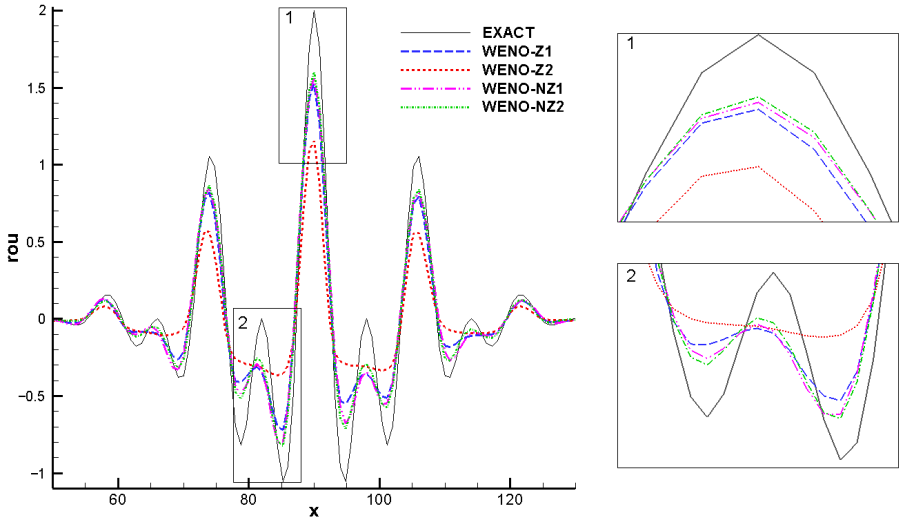

Figure 6. Numerical solutions of linear advection problem with several critical points computed by different WENO schemes.

4.2.1. SOD Problem

The initial conditions of the sod problem are as follows

$$(, u, p) = \begin{cases} (1, 0, 1), & 0 \le x < 0.5, \\ (0.125, 0, 0.1), & 0.5 \le x \le 1. \end{cases} \tag{35}$$

This problem is run up to the final time $t = 0.25$ with $N = 200$, resulting in a shock wave, a contact discontinuity, and an expansion wave. From Figure 7a, all the schemes can both simulate the sod problem without oscillatory. The zoom-in results of contact discontinuity for different schemes are displayed in Figure 7b. It can be found that the WENO-NZ1 scheme can capture the contact discontinuities well and is slightly closer to the "exact" solution than the others.

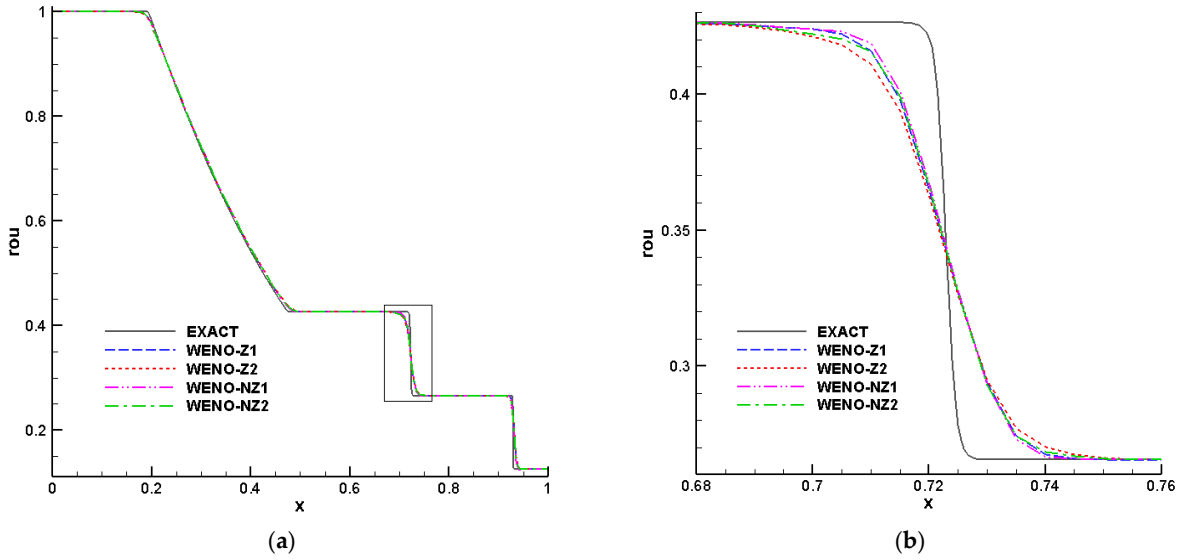

Figure 7. Numerical solutions of sod problem computed by different schemes; (**a**) density distribution; (**b**) a zoom of contact discontinuity.

4.2.2. Lax Problem

The initial conditions of the lax problem are as follows

$$(\rho,\ u,\ p) = \begin{cases} (0.445,\ 0.698,\ 0.3528), & -5 \le x < 0, \\ (0.5,\ 0,\ 0.571), & 0 \le x \le 5. \end{cases} \tag{36}$$

Figure 8 shows a comparison of different schemes with $N = 200$ at $t = 1.3$. From Figure 8a, we can see that all schemes can pass through the sound velocity point smoothly. However, it can be seen from Figure 8b that, in comparison to WENO-Z, the corresponding WENO-NZ scheme provides lower numerical dissipation.

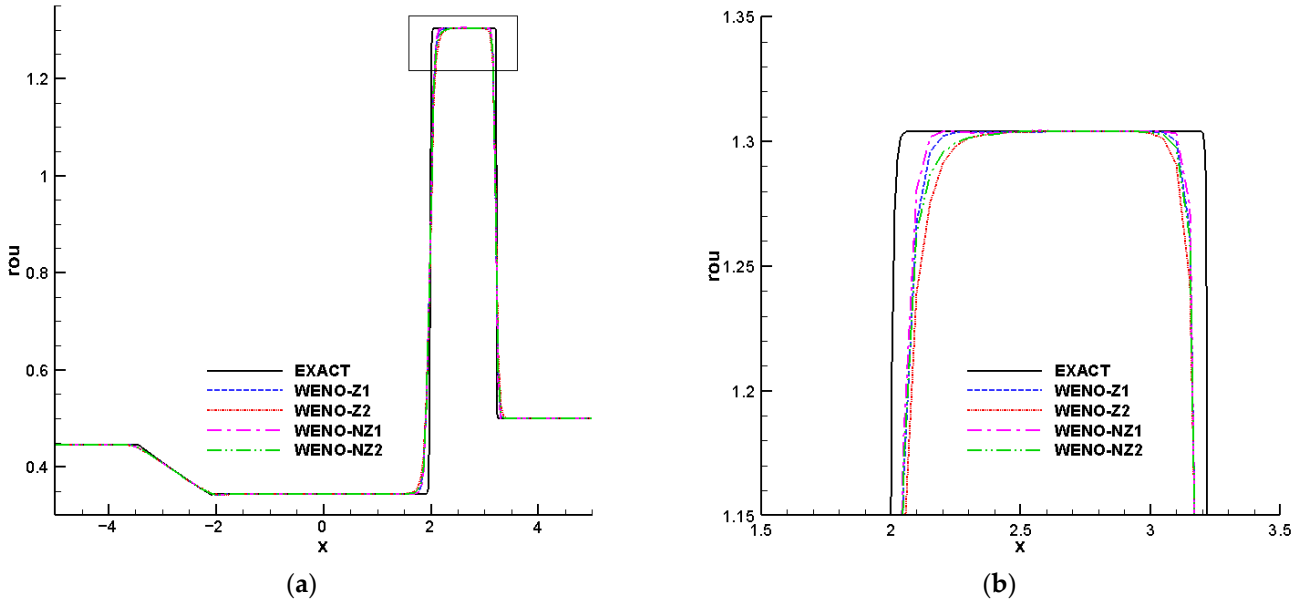

Figure 8. Numerical solutions of lax problem computed by different schemes; (**a**) density distribution; (**b**) a zoom of discontinuity.

4.2.3. Shu–Osher Problem

The initial conditions of Shu–Osher shock-entropy wave interaction are as follows

$$(\rho,\ u,\ p) = \begin{cases} (3.857143,\ 2.629369,\ 10.33333), & -5 \le x < -4, \\ (1 + 0.2sin(5\,x),\ 0,\ 1.0), & -4 \le x \le 5. \end{cases} \tag{37}$$

This problem involves the presence of shocklets and fine-scale structures, it is frequently utilized to study the stability of capturing shocks. We solve this problem until $t = 1.8$ using $N = 200$ and present the density results for different schemes in Figure 9. Examining the high-frequency wave region as depicted in Figure 9b, it can be seen that the WENO-NZ scheme performs a better job in approaching the "exact" solution compared to WENO-Z. Especially, in the area [1.3, 2.3], the numerical dissipation of WENO-NZ2 is even equivalent to WENO-NZ1. Based on the observations from Figures 7–9, it can be concluded that the proposed WENO-NZ scheme effectively reduces numerical dissipation and is capable of stable shock capture.

4.3. Two-Dimensional Euler Problems

The two-dimensional Euler equation can be written as

$$\frac{\partial \mathbf{U}}{\partial t} + \frac{\partial \mathbf{F}(\mathbf{U})}{\partial x} + \frac{\partial \mathbf{G}(\mathbf{U})}{\partial y} = 0, \tag{38}$$

with

$$\mathbf{U} = \begin{pmatrix} \rho \\ \rho u \\ \rho v \\ E \end{pmatrix}, \ \mathbf{F}(\mathbf{U}) = \begin{pmatrix} \rho u \\ \rho u^2 + p \\ \rho uv \\ u(E+p) \end{pmatrix}, \ \mathbf{G}(\mathbf{U}) = \begin{pmatrix} \rho v \\ \rho uv \\ \rho v^2 + p \\ v(E+p) \end{pmatrix}. \tag{39}$$

Here, ρ, p, u, and v are the density, pressure, x- and y-velocity, respectively. The total energy E is given as $E = \frac{p}{\gamma-1} + \frac{1}{2}\rho(u^2+v^2)$ with the ratio of specific heat $\gamma = 1.4$, unless otherwise indicated.

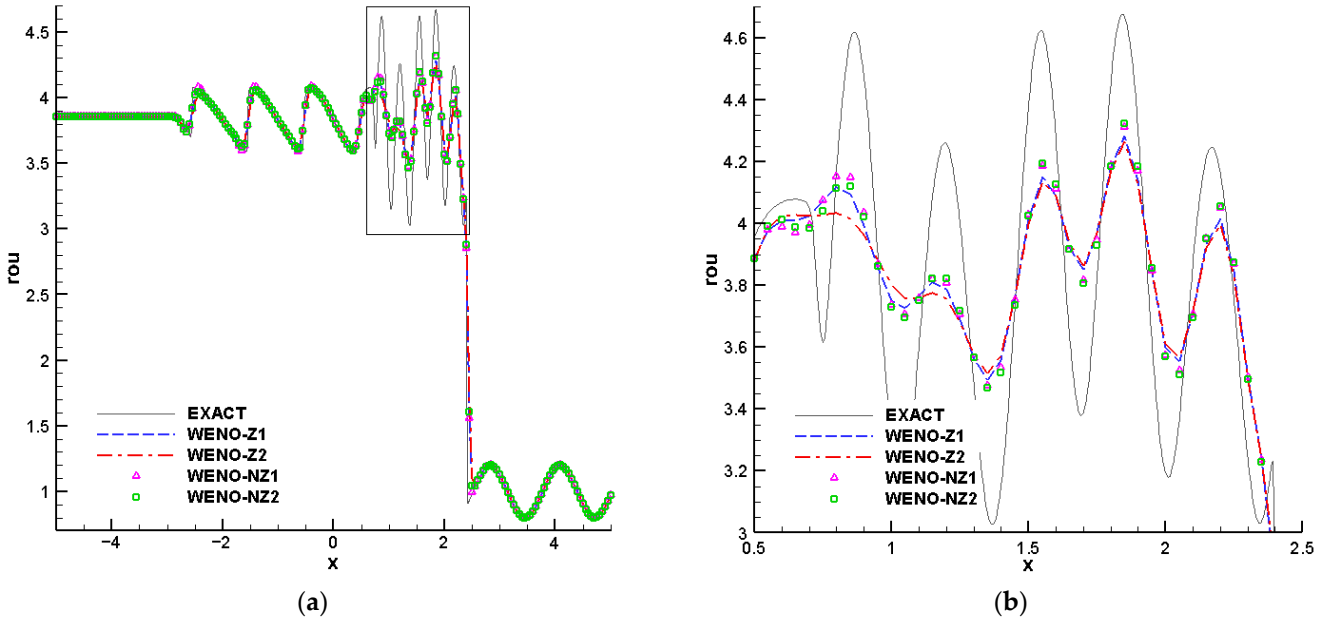

Figure 9. Numerical solutions of the Shu-Osher problem computed by different schemes; (**a**) density distribution; (**b**) a zoom of the high-frequency wave.

4.3.1. Riemann Problem

The initial conditions of the two-dimensional Riemann problem are as follows

$$(\rho,\, u,\, v,\, p) = \begin{cases} (1.5,\, 0,\, 0,\, 1.5), & 0.8 \le x \le 1,\ 0.8 \le y \le 1, \\ (0.5323,\, 1.206,\, 0,\, 0.3), & 0 \le x < 0.8,\ 0.8 \le y \le 1, \\ (0.138,\, 1.206,\, 1.206,\, 0.029), & 0 \le x < 0.8,\ 0 \le y < 0.8, \\ (0.5323,\, 0,\, 1.206,\, 0.3), & 0.8 \le x \le 1,\ 0 \le y < 0.8. \end{cases} \tag{40}$$

With the computational domain $[0,1] \times [0,1]$, this problem involves some vortex structures generated by Kelvin–Helmholtz instability and is often used to investigate numerical dissipation. Figure 10 gives the density profiles computed by different schemes at $t = 0.3$ with uniform meshes of 800×800 and zero-order extrapolation boundary conditions. As depicted in the results, the WENO-NZ scheme captures reflected shock waves more accurately and clearly than WENO-Z, which indicates that the numerical dissipation of WENO-NZ is smaller than that of WENO-Z. Among these schemes, WENO-NZ1 exhibits the richest vortex structures. However, it is important to note that when the time is pushed forward to longer, WENO-NZ1 will break the symmetrical roll-up of the Kelvin–Helmholtz instability because its numerical dissipation is too small. Fortunately, WENO-NZ2 not only performs well but also can maintain symmetry to solve this problem.

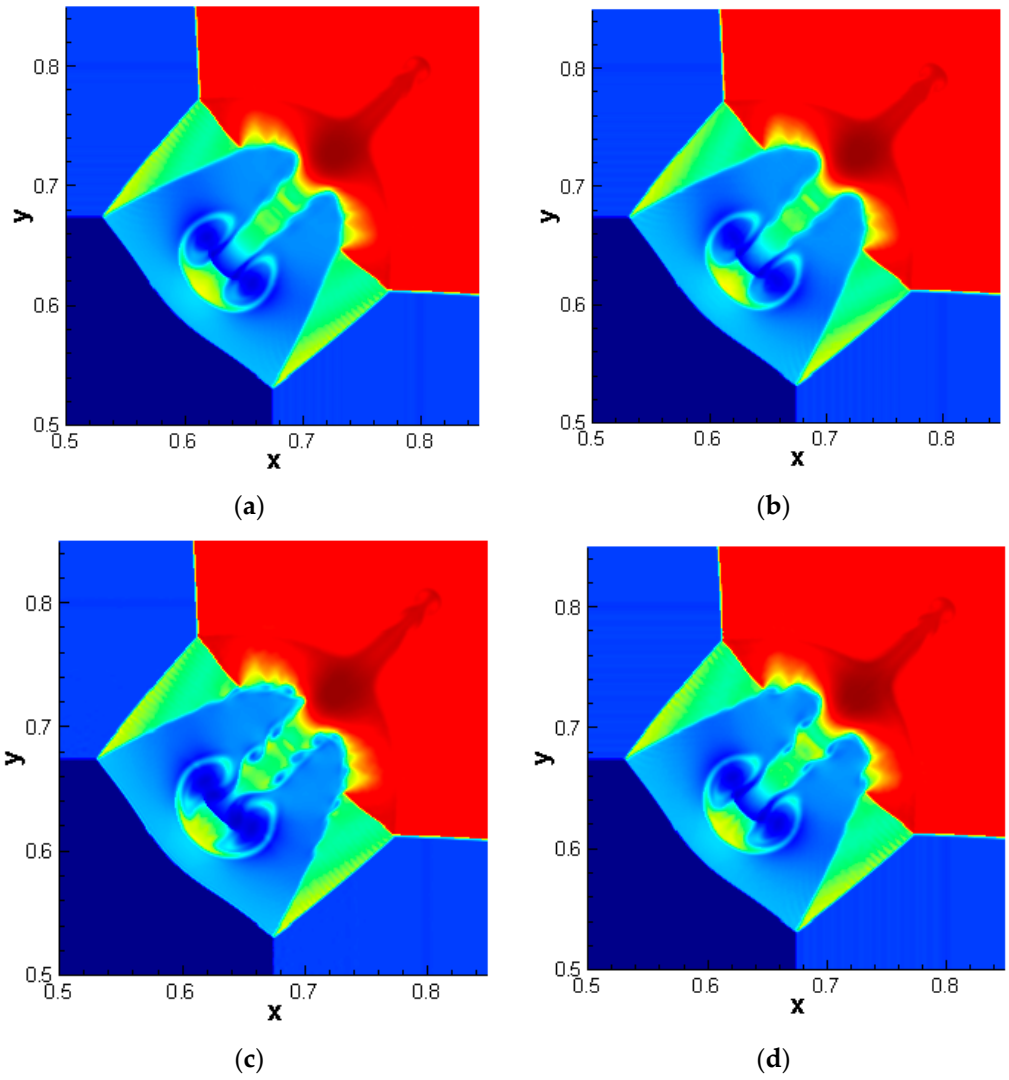

Figure 10. Numerical solutions of 2D Riemann problem computed by different schemes; (**a**) WENO-Z1; (**b**) WENO-Z2; (**c**) WENO-NZ1; (**d**) WENO-NZ2.

4.3.2. Double Mach Reflection Problem

The double Mach reflection problem depicts a right-moving Mach 10 shock wave with an angle of 60° hitting a reflecting wall at $x = 1/6$, which lies at the bottom of the computational domain $[0, 4] \times [0, 1]$. This results in the formation of complex flow patterns, including shock wave reflections and vortex structures (see Figure 11, which is computed by the WENO-Z1 scheme using grids 960×240 to $t = 0.25$). The initial conditions are as follows

$$(\rho, u, v, p) = \begin{cases} (1.4, 0, 0, 1), & y < \sqrt{3}(x - 1/6), \\ (8, 7.145, -4.125, 116.833), & y \geq \sqrt{3}(x - 1/6). \end{cases} \tag{41}$$

The exact post shock condition is imposed from $x = 0$ to $x = 1/6$ and the reflective boundary condition is used for the rest of the bottom. The boundary condition at the top corresponds to the exact motion of a Mach 10 shock, while the left and right boundaries are subject to inflow and outflow boundary conditions, respectively. Figure 12 shows the density results near the Mach stem computed by different schemes with uniform meshes of 960×240. It can be seen that the WENO-NZ scheme depicts richer vortex structures and has a higher resolution compared with the WENO-Z scheme. In addition, Figure 13 further shows the local density profiles computed by using denser meshes of 1600×400, it

can be also seen that the WENO-NZ scheme still performs better results than WENO-Z. However, Figures 12 and 13 both show that WENO-NZ1 exhibits Gibbs oscillation due to its numerical dissipation being too small, while WENO-NZ2 does not. Based on the numerical results of the Riemann problem and double Mach reflection problem, it is not difficult to find that the numerical dissipation is too small and would not be a good choice for some two-dimensional problems involving small vortex structures, so we suggest taking the power to be $q = 2$ for WENO-NZ to calculate these problems.

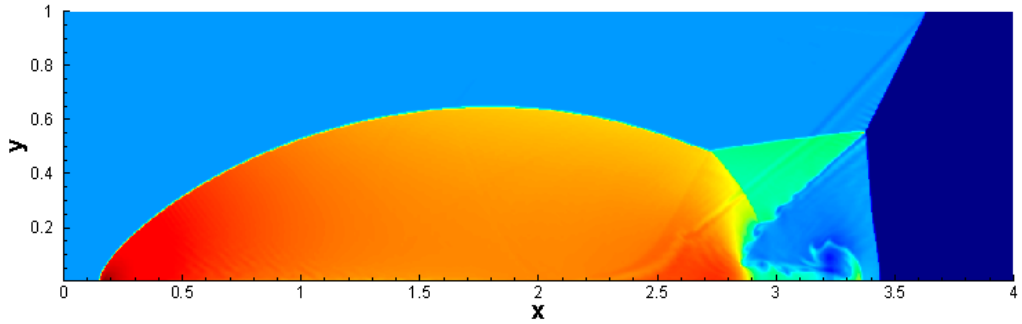

Figure 11. Numerical solutions of double Mach reflection problem computed by the WENO-Z1 scheme with uniform meshes of 960×240.

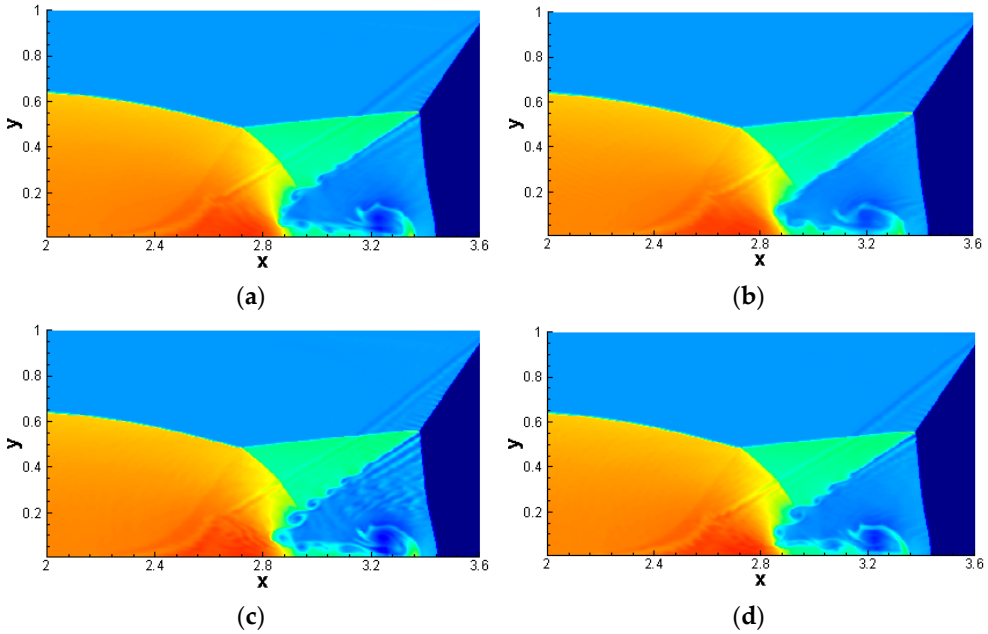

Figure 12. A zoom of numerical solutions near the Mach stem for the double Mach reflection problem, which is computed by different schemes with uniform meshes of 960×240; (**a**) WENO-Z1; (**b**) WENO-Z2; (**c**) WENO-NZ1; (**d**) WENO-NZ2.

4.3.3. Rayleigh–Taylor Instability Problem

The Rayleigh–Taylor instability problem describes the interface instability when a heavy fluid accelerates into a light one, whose initial conditions are given as

$$(\rho,\, u,\, v,\, p) = \begin{cases} \left(2,\, 0,\, -0.025\sqrt{\gamma p/\rho}\cos(8\pi x),\, 2y+1\right), & 0 \le y < 0.5, \\ \left(1,\, 0,\, -0.025\sqrt{\gamma p/\rho}\cos(8\pi x),\, y+1.5\right), & 0.5 \le y \le 1. \end{cases} \tag{42}$$

The computational domain is $[0, 0.25] \times [0, 1]$ and the ratio of specific heat is $\gamma = 5/3$. The reflective boundary conditions are employed for the left and right boundaries. The

boundary conditions on the top and bottom boundaries are given as $(\rho, u, v, p) = (1, 0, 0, 2.5)$ and $(\rho, u, v, p) = (2, 0, 0, 1)$, respectively. Figure 14 gives the density results computed by different schemes with meshes of 240 × 960 until t = 1.95. It is apparent that all schemes are able to maintain the symmetry of the growth of instability. Compared to WENO-Z, the proposed WENO-NZ scheme displays more finer microstructures. Figure 15 further gives the density results computed to t = 1.95 by using denser meshes of 400 × 1600. Obviously, the WENO-NZ scheme exhibits a greater richness of complex vortex structures and better resolution than the WENO-Z scheme.

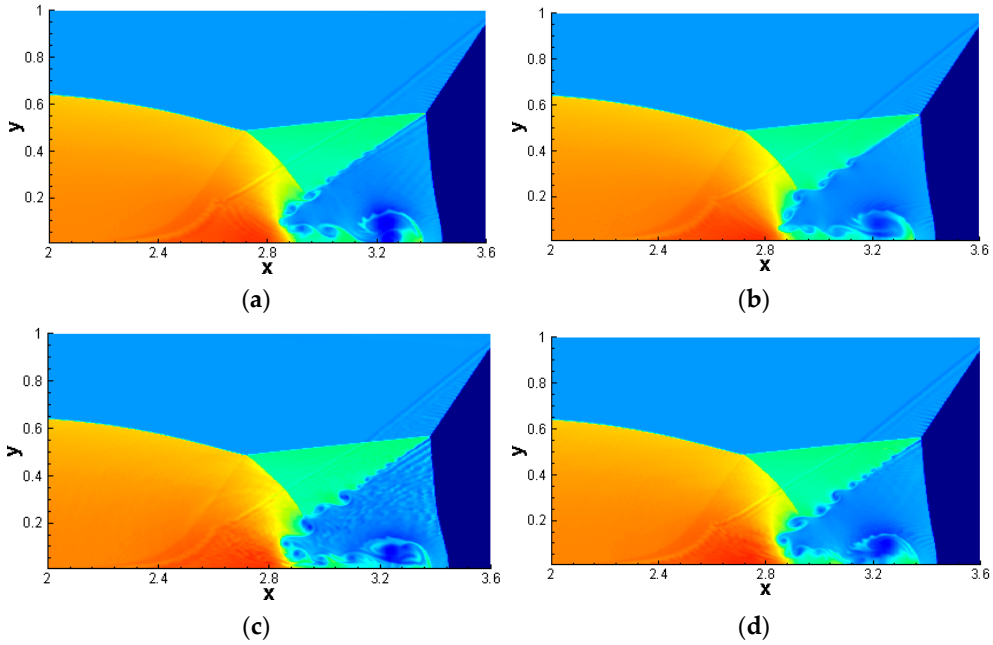

Figure 13. A zoom of numerical solutions near the Mach stem for the double Mach reflection problem, which is computed by different schemes with uniform meshes of 1600 × 400; (**a**) WENO-Z1; (**b**) WENO-Z2; (**c**) WENO-NZ1; (**d**) WENO-NZ2.

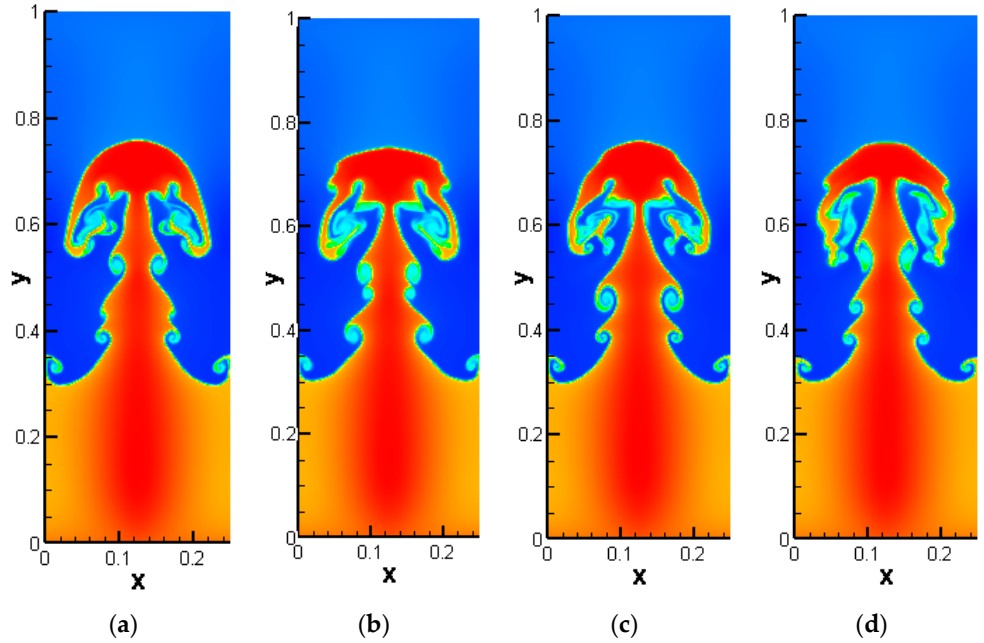

Figure 14. Numerical solutions of Rayleigh–Taylor instability problem computed by different schemes with uniform meshes of 240 × 960; (**a**) WENO-Z1; (**b**) WENO-Z2; (**c**) WENO-NZ1; (**d**) WENO-NZ2.

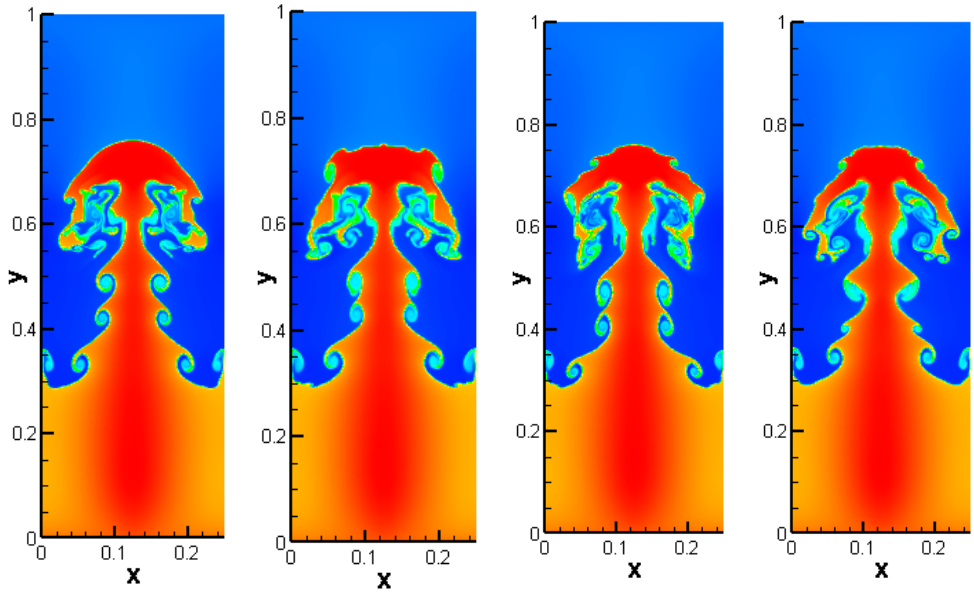

Figure 15. Numerical solutions of Rayleigh–Taylor instability problem computed by different schemes with uniform meshes of 400 × 1600; (**a**) WENO-Z1; (**b**) WENO-Z2; (**c**) WENO-NZ1; (**d**) WENO-NZ2.

5. Conclusions

In this study, we modified the global smoothness indicator of the fifth-order WENO-Z scheme to improve its performance. First, the five-point global stencil was subdivided into four smaller sub-stencils that are usually used to construct the third-order WENO-Z scheme. Based on these lower-order smoothness indicators, a novel global smoothness indicator with fifth-order accuracy was reconstructed, which resulted in the new WENO-NZ scheme. The results from ADR analysis implied that the proposed scheme was a low-dissipation scheme, whatever the value of power q. Accuracy tests showed that the WENO-NZ scheme with either $q = 1$ or $q = 2$ could achieve fifth-order accuracy even at critical points. Compared with the WENO-Z scheme, although the WENO-NZ had the same theoretical convergence accuracy, the WENO-Z failed to balance the low-dissipation property and fifth-order convergence. Moreover, a series of one- and two-dimensional benchmark problems demonstrated the WENO-NZ scheme showed lower numerical dissipation and better resolution than WENO-Z. However, for some two-dimensional problems involving small vortex structures, the power q was best to be 2 for the WENO-NZ scheme since the numerical dissipation was too small to suppress oscillation when $q = 1$.

Author Contributions: Conceptualization, S.H. and M.L.; methodology, S.H. and M.L.; software, S.H.; validation, S.H.; formal analysis, S.H. and M.L.; investigation, S.H.; resources, S.H.; data curation, S.H.; writing—original draft preparation, S.H.; writing—review and editing, S.H. and M.L.; visualization, S.H.; supervision, M.L.; project administration, M.L.; funding acquisition, M.L. All authors have read and agreed to the published version of the manuscript.

Funding: This research was funded by National Natural Science Foundation of China under grant no. (11971411).

Data Availability Statement: Not applicable.

Conflicts of Interest: The authors declare no conflict of interest.

References

1. Harten, A. High resolution schemes for hyperbolic conservation laws. *J. Comput. Phys.* **1983**, *49*, 357–393. [CrossRef]
2. Toro, E.F.; Billett, S.J. Centred TVD schemes for hyperbolic conservation laws. *IMA J. Numer. Anal.* **2000**, *20*, 47–79. [CrossRef]
3. Tang, S.J.; Li, M.J. Construction and application of several new symmetrical flux limiters for hyperbolic conservation law. *Comput. Fluids* **2020**, *93*, 104741. [CrossRef]
4. Harten, A.; Osher, S.; Engquist, B.; Chakravarthy, S.R. Some results on uniformly high-order accurate essentially nonoscillatory schemes. *Appl. Numer. Math.* **1986**, *2*, 347–377. [CrossRef]
5. Harten, A.; Engquist, B.; Osher, S.; Chakravarthy, S.R. Uniformly high order accurate essentially non-oscillatory schemes, III. *J. Comput. Phys.* **1987**, *71*, 231–303. [CrossRef]
6. Shu, C.W.; Osher, S. Efficient implementation of essentially non-oscillatory shock-capturing schemes. *J. Comput. Phys.* **1988**, *77*, 439–471. [CrossRef]
7. Liu, X.D.; Osher, S.; Chan, T. Weighted essentially non-oscillatory schemes. *J. Comput. Phys.* **1994**, *115*, 200–212. [CrossRef]
8. Jiang, G.S.; Shu, C.W. Efficient implementation of weighted ENO schemes. *J. Comput. Phys.* **1996**, *126*, 202–228. [CrossRef]
9. Borges, R.; Carmona, M.; Costa, B.; Don, W.S. An improved weighted essentially non-oscillatory scheme for hyperbolic conservation laws. *J. Comput. Phys.* **2008**, *227*, 3191–3211. [CrossRef]
10. Tang, S.J.; Li, M.J. Novel functional weights for improving the third-order WENO schemes. *Int. J. Numer. Meth. Fluids* **2021**, *93*, 3131–3150. [CrossRef]
11. Henrick, A.K.; Aslam, T.D.; Powers, J.M. Mapped weighted essentially non-oscillatory schemes: Achieving optimal order near critical points. *J. Comput. Phys.* **2005**, *207*, 542–567. [CrossRef]
12. Guo, J.; Jung, J.H. Radial basis function ENO and WENO finite difference methods based on the optimization of shape parameters. *J. Sci. Comput.* **2017**, *70*, 551–575. [CrossRef]
13. Guo, J.; Jung, J.H. A RBF-WENO finite volume method for hyperbolic conservation laws with the monotone polynomial interpolation method. *Appl. Numer. Math.* **2017**, *112*, 27–50. [CrossRef]
14. Abedian, R. A finite difference Hermite RBF-WENO scheme for hyperbolic conservation laws. *Int. J. Numer. Meth. Fluids* **2022**, *94*, 583–607. [CrossRef]
15. Abedian, R.; Dehghan, M. The formulation of finite difference RBFWENO schemes for hyperbolic conservation laws: An alternative technique. *Adv. Appl. Math. Mech.* **2023**, *15*, 1023–1055. [CrossRef]
16. Zeng, F.J.; Shen, Y.Q.; Liu, S.P. A perturbational weighted essentially non-oscillatory scheme. *Comput. Fluids* **2018**, *172*, 196–208. [CrossRef]
17. Castro, M.; Costa, B.; Don, W.S. High order weighted essentially non-oscillatory WENO-Z schemes for hyperbolic conservation laws. *J. Comput. Phys.* **2011**, *230*, 1766–1792. [CrossRef]
18. Cheng, X.H.; Feng, J.H.; Zheng, S.P. A fourth order WENO scheme for hyperbolic conservation laws. *Adv. Appl. Math. Mech.* **2020**, *12*, 992–1007. [CrossRef]
19. Xu, W.Z.; Wu, W.G. An improved third-order weighted essentially non-oscillatory scheme achieving optimal order near critical points. *Comput. Fluids* **2018**, *162*, 113–125. [CrossRef]
20. Wang, Y.H.; Du, Y.L.; Zhao, K.L.; Li, Y. A low-dissipation third-order weighted essentially nonoscillatory scheme with a new reference smoothness indicator. *Int. J. Numer. Meth. Fluids* **2020**, *92*, 1212–1234. [CrossRef]
21. Kim, C.H.; Ha, Y.; Yoon, J. Modified non-linear weights for fifth-order weighted essentially non-oscillatory schemes. *J. Sci. Comput.* **2016**, *67*, 299–323. [CrossRef]
22. Rathan, S.; Gande, N.R.; Bhise, A.A. Simple smoothness indicator WENO-Z scheme for hyperbolic conservation laws. *Appl. Numer. Math.* **2020**, *157*, 255–275. [CrossRef]
23. Liu, S.P.; Shen, Y.Q.; Zeng, F.J.; Ming, Y. A new weighting method for improving the WENO-Z scheme. *Int. J. Numer. Meth. Fluids* **2018**, *87*, 271–291. [CrossRef]
24. Acker, F.; Borges, R.; Costa, B. An improved WENO-Z scheme. *J. Comput. Phys.* **2016**, *313*, 726–753. [CrossRef]
25. Tang, S.J.; Feng, Y.J.; Li, M.J. Novel weighted essentially non-oscillatory schemes with adaptive weights. *Appl. Math. Comput.* **2022**, *420*, 126893. [CrossRef]
26. Don, W.S.; Borges, R. Accuracy of the weighted essentially non-oscillatory conservative finite difference schemes. *J. Comput. Phys.* **2013**, *250*, 347–372. [CrossRef]
27. Pirozzoli, S. On the spectral properties of shock-capturing scheme. *J. Comput. Phys.* **2006**, *219*, 489–497. [CrossRef]